

FLOW MATCHING FOR POSTERIOR INFERENCE WITH SIMULATOR FEEDBACK

Benjamin Holzsuh, Nils Thuerey

School for Computation, Information and Technology

Technical University of Munich

{benjamin.holzsuh, nils.thuerey}@tum.de

ABSTRACT

Flow-based generative modeling is a powerful tool for solving inverse problems in physical sciences that can be used for sampling and likelihood evaluation with much lower inference times than traditional methods. We propose to refine flows with additional control signals based on a simulator. Control signals can include gradients and a problem-specific cost function if the simulator is differentiable, or they can be fully learned from the simulator output. In our proposed method, we pretrain the flow network and include feedback from the simulator exclusively for finetuning, therefore requiring only a small amount of additional parameters and compute. We motivate our design choices on several benchmark problems for simulation-based inference and evaluate flow matching with simulator feedback against classical MCMC methods for modeling strong gravitational lens systems, a challenging inverse problem in astronomy. We demonstrate that including feedback from the simulator improves the accuracy by 53%, making it competitive with traditional techniques while being up to 67x faster for inference. Code and experiments are available at <https://github.com/tum-pbs/sbi-sim>.

1 INTRODUCTION

Acquiring posterior distributions given measurement data is of paramount scientific interest (Cranmer et al., 2020), with real-world applications ranging from particle physics (Baydin et al., 2019), over the inference of gravitational waves (Dax et al., 2021) to predictions of dynamical systems such as weather forecasting (Gneiting & Raftery, 2005). For an observation x_o and model parameters θ , the likelihood $p(x_o|\theta)$ corresponds to how strongly we believe a model with parameters θ causes x_o to occur. In Bayesian modeling, we are interested in the posterior $p(\theta|x_o)$, which is proportional to the likelihood times the prior $p(\theta)$ and tells us which parameters most likely explain the observation.

Inferring the posterior based on samples from traditional likelihood-based methods can be expensive for high-dimensional data and when likelihood evaluations are costly. Simulation-based inference (Cranmer et al., 2020, SBI) represents the posterior as a parametric function $q(\theta|x_o)$, which is a learnable conditional density estimator that can be trained purely by simulations $x \sim p(x|\theta)$ alone. By investing an upfront cost for training the density estimator, we can sample and compute likelihoods from $q(\theta|x_o)$ much faster than other methods, thereby amortizing the training cost over many observations.

Traditionally, normalizing flows (Rezende & Mohamed, 2015; Dinh et al., 2017; Papamakarios et al., 2019) have been a popular class of density estimators used in many areas of science. To compute likelihoods and for sampling, normalizing flows transform a noise distribution to the posterior distribution. With the success of diffusion models Ho et al. (2020); Liu et al. (2023); Lipman et al. (2023), it became clear that the mapping between sampling and posterior distribution can be specified a priori, for example by specifying a corruption process that transforms any data distribution to a normal Gaussian. The resulting continuous-time models outperform discrete architecture in many areas, and training larger models is much more scalable.

Despite the widespread success of flow-based models for generative modeling and density estimation, there is no direct feedback loop between the model, the observation x_o and the sample θ during training, which makes it very difficult to produce highly accurate samples based on learning alone.

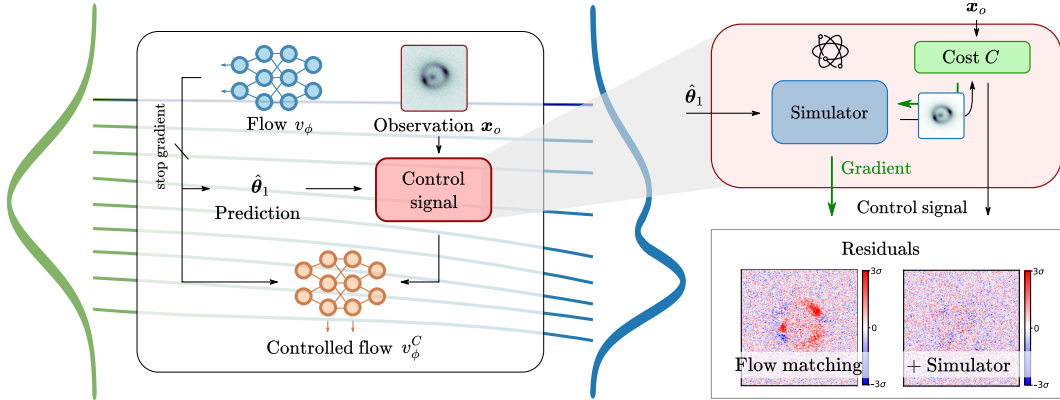


Figure 1: An overview of our proposed framework. We consider a pretrained flow network v_ϕ and use the predicted flow for the trajectory point θ_t at time t to estimate $\hat{\theta}_1$. On the right, we show a gradient-based control signal with a differentiable simulator and cost function C for improving $\hat{\theta}_1$. An additional network learns to combine the predicted flow with feedback via the control signal to give a new controlled flow. By combining learning-based updates with suitable controls, we avoid local optima and obtain high-accuracy samples with low inference times.

We propose a simple strategy to reintroduce control signals using **simulators** into the flow network. We refine an existing pretrained flow-based model with a flexible control signal by aggregating the learned flow and control signals into a *controlled flow*. The aggregation network is small compared to the pretrained flow network, and we find that freezing the weights of the pretrained network works very well; thus, refining needs only a minimal amount of additional parameters and compute.

To demonstrate how these refinements affect the accuracy of samples and the posterior, we consider modeling strong gravitational lens systems (Hezaveh et al., 2017; Cunha & Herdeiro, 2018; Legin et al., 2021; Vegetti & Koopmans, 2009; Vegetti et al., 2023), an inverse problem in astrophysics that is challenging and requires precise posteriors for accurate modeling of observations. In galaxy-scale strong lenses, light from a source galaxy is deflected by the gravitational potential of a galaxy between the source and observer, causing multiple images of the source to be seen. Since these images and their distortions are sensitive to the distribution of matter on small scales, this can act as a probe for different dark matter models. With upcoming and current sky surveys (Laureijs et al., 2011) expected to release large data catalogs in the near future, the number of known lenses will increase dramatically by several orders of magnitude. Traditional computational approaches require several minutes to many hours or days to model a single lens system. Therefore, there is an urgent need to reduce the compute and inference with learning-based methods. In this experiment, we demonstrate that using flow matching and our proposed control signals with feedback from a simulator, we obtain posterior distributions for lens modeling that are competitive with the posteriors obtained by MCMC-based methods but with much faster inference times.

Additionally, we evaluate different related variants of flow matching such as independent couplings (Tong et al., 2023), self-conditioning (Chen et al., 2023) or different loss formulations in the context of SBI using several benchmark problems. We then analyze our proposed control signals for the Lotka-Volterra model, a system of coupled ordinary differential equations (ODEs) describing the population evolution of predators and prey over time. Our analysis underscores the essential role of simulator feedback for inference and that high accuracy is very challenging to achieve from scaling up datasets and model sizes alone.

To summarize, the main contributions of our work are:

- We propose a versatile strategy to improve pretrained flows with control signals based on feedback from a simulator. Control signals can be based on gradients and a cost function, if the simulator is differentiable, but they can also be learned directly from the simulator output.
- We assess different variants of flow matching in the context of SBI and demonstrate with the Lotka-Volterra model that performance gains due to simulator feedback are substantial and cannot be achieved by training on larger datasets alone.

- We demonstrate the efficacy of our proposed finetuning with control signals for inferring the parameter distributions of strong gravitational lens systems, a challenging inverse problem in astronomy that is sensitive to sample accuracy. We show that flow matching with simulator feedback is competitive with MCMC baselines and beats them significantly regarding inference time.

2 RELATED WORK

Solving inverse problems with diffusion models Diffusion models have been proposed to solve linear inverse problems (Kawar et al., 2021; 2022; Chung et al., 2022; Cardoso et al., 2023), as well as general inverse problems (Holzschuh et al., 2023; Chung et al., 2023a;b). In most of these works, the diffusion model learns the prior distribution and sampling from the posterior is achieved through a modified inference procedure, which guides samples via a conditioning. The conditioning can be based on a class label, text input (Song et al., 2021; Ho & Salimans, 2022; Saharia et al., 2022; Wu et al., 2023) or directly on a differentiable measurement operator (Chung et al., 2023a;b). In contrast to these works, we finetune a pretrained flow and learn an optimal combination of the pretrained flow and feedback from a simulator via control signals in the broader flow matching context.

Flow matching Our work builds on top of prior work in flow matching (Lipman et al., 2023; Albergo et al., 2023a; Pooladian et al., 2023; Tong et al., 2023; Albergo et al., 2023b), particularly we adopt and evaluate conditional optimal transport paths (Lipman et al., 2023) and independent couplings or rectified flows (Liu et al., 2023; Tong et al., 2023) for simulation-based inference. We extend the existing literature by adding feedback from a simulator for scientific inverse problems.

Simulation-based inference Our work directly compares to neural posterior estimation approaches for simulation-based inference (Cranmer et al., 2020; Lueckmann et al., 2021, SBI). Contrary to static architectures (Dinh et al., 2017; Kingma & Dhariwal, 2018; Papamakarios et al., 2017; Durkan et al., 2019), our approach extends the continuous-time paradigm (Chen et al., 2018; Grathwohl et al., 2019). Wildberger et al. (2023) have applied flow matching to neural posterior estimation and Sharrock et al. (2022) have used conditional diffusion models and Langevin dynamics during sampling. In contrast to previous work, we include controls signals via problem-specific simulators and cost functions during training to significantly improve the sampling quality.

Strong lensing and parameter estimation Machine learning has been successfully applied to estimate parameters of lens and source models (Hezaveh et al., 2017; Levasseur et al., 2017), however, previous methods are usually restricted to point estimates, use simple variational distributions or Bayesian Neural Networks (Schuldt et al., 2021; Legin et al., 2021; 2023; Poh et al., 2022) that are not well suited to represent more complicated high-dimensional data distributions. In this paper, we combine flow matching with problem-specific simulators to obtain highly accurate samples via feedback from control signals.

3 FLOW MATCHING THEORY

Continuous-time flow models transform samples θ from a sampling distribution p_0 to samples of a target or posterior distribution p_1 . This mapping can be expressed via the ODE

$$d\theta_t = v_\theta(t, \theta_t)dt, \quad (1)$$

where $v_\phi(t, \theta_t)$ represents a neural network with parameters ϕ . Early works (Chen et al., 2018; Grathwohl et al., 2019) optimize $v_\phi(t, \theta)$ using maximum likelihood training, which is computationally demanding and difficult to scale to larger networks. Instead, in flow matching the network $v_\phi(t, \theta)$ is trained by regressing a vector field $u(t, \theta)$ that generates probability paths that map from p_0 to p_1 .

Generating probability paths We say that a smooth vector field $u : [0, 1] \times \mathbb{R}^d \rightarrow \mathbb{R}^d$, called *velocity*, generates the probability paths p_t , if it satisfies the continuity equation $\frac{\partial p}{\partial t} = -\nabla \cdot (p_t u_t)$. Informally, this means that we can sample from the distribution p_t by sampling $\theta_0 \sim p_0$ and then solving the ODE $d\theta = u(t, \theta)dt$ with initial condition θ_0 . In the following, we will denote $u(t, \theta)$ by $u_t(\theta)$. To regress the velocity field, we define the **flow matching** objective

$$\mathcal{L}_{\text{FM}}(\theta) := \mathbb{E}_{t \sim \mathcal{U}(0,1), \theta \sim p_t(\theta)} \|v_\theta(t, \theta) - u_t(\theta)\|^2. \quad (2)$$

In order to compute this loss, we need to sample from the probability distribution $p_t(\boldsymbol{\theta})$ and we need to know the velocity $u_t(\boldsymbol{\theta})$. However, in general $u_t(\boldsymbol{\theta})$ is not accessible.

Conditioning variable To solve this problem, we apply a trick by introducing a latent variable \mathbf{z} distributed according to $q(\mathbf{z})$ and define the conditional likelihoods $p_t(\boldsymbol{\theta}|\mathbf{z})$ that depend on the latent variable so that $p_t(\boldsymbol{\theta}) = \int p_t(\boldsymbol{\theta}|\mathbf{z})q(\mathbf{z})d\mathbf{z}$. Interestingly, if the conditional likelihoods are generated by the velocities $u_t(\boldsymbol{\theta}|\mathbf{z})$, then the velocity $u_t(\boldsymbol{\theta})$ can be written in terms of $u_t(\boldsymbol{\theta}|\mathbf{z})$ and $p_t(\boldsymbol{\theta}|\mathbf{z})$ with $u_t(\boldsymbol{\theta}) := \mathbb{E}_{q(\mathbf{z})}[u_t(\boldsymbol{\theta}|\mathbf{z})p_t(\boldsymbol{\theta}|\mathbf{z})/p_t(\boldsymbol{\theta})]$. We can choose paths $p_t(\boldsymbol{\theta}|\mathbf{z})$ that are easy to sample from and for which we know the generating velocities $u_t(\boldsymbol{\theta}|\mathbf{z})$. Next, we define the **conditional flow matching** loss

$$\mathcal{L}_{\text{CFM}}(\phi) := \mathbb{E}_{t,q(\mathbf{z}),p_t(\boldsymbol{\theta}|\mathbf{z})} \|v_\phi(t, \boldsymbol{\theta}) - u_t(\boldsymbol{\theta}|\mathbf{z})\|^2. \quad (3)$$

In contrast to the flow matching loss eq. 2, this loss is tractable and can be used for optimization. Now, one can show (Tong et al., 2023) that if $p_t(\boldsymbol{\theta}) > 0$ for all $\boldsymbol{\theta} \in \mathbb{R}^d$, then

$$\nabla_\phi \mathcal{L}_{\text{FM}}(\phi) = \nabla_\phi \mathcal{L}_{\text{CFM}}(\phi). \quad (4)$$

This means that we can train $v_\phi(\boldsymbol{\theta}, t)$ to regress $u_t(\boldsymbol{\theta})$ generating the mapping between p_0 and p_1 by optimizing the conditional flow matching loss eq. 3.

Couplings The above framework allows for many degrees of freedom when specifying the mapping from p_0 to p_1 via the conditioning variable \mathbf{z} and the conditional likelihoods p_t . One particularly intuitive and simple choice is to consider the coupling $q(\mathbf{z}) = p_1(\boldsymbol{\theta})$ (Lipman et al., 2023) together with conditional probability and generating velocity

$$p_t(\boldsymbol{\theta}|\boldsymbol{\theta}_1) = \mathcal{N}(\boldsymbol{\theta}|t\boldsymbol{\theta}_1, (1 - (1 - \sigma_{\min})t)I) \quad (5)$$

$$u_t(\boldsymbol{\theta}|\boldsymbol{\theta}_1) = \frac{\boldsymbol{\theta}_1 - (1 - \sigma_{\min})\boldsymbol{\theta}}{1 - (1 - \sigma_{\min})t}, \quad (6)$$

where $\sigma_{\min} > 0$. Conditioned on $\boldsymbol{\theta}_1$, this coupling transports a point $\boldsymbol{\theta}_0 \sim \mathcal{N}(0, I)$ from the sampling distribution to the posterior distribution on the linear trajectory $t\boldsymbol{\theta}_1$ ending in $\boldsymbol{\theta}_1$ but decreasing the standard deviation from 1 to a smoothing constant σ_{\min} . In this case, the transport path coincides with the optimal transport between two Gaussian distributions.

4 CONTROLS FOR IMPROVED ACCURACY

While flow-based models $v_\phi(t, \boldsymbol{\theta})$ gradually transform samples from p_0 to p_1 in many steps during inference via solving the ODE eq. 1, there is no direct feedback loop between the underlying simulator, the current point on the trajectory $\boldsymbol{\theta}_t$, and the observation \mathbf{x}_o . A central goal of our work is to reintroduce this feedback loop into inference and training by incorporating a control signal.

Conditioning of flows Flows $v_\phi(t, \boldsymbol{\theta})$ can be conditioned on an observation \mathbf{x}_o through an additional input $v_\phi(t, \boldsymbol{\theta}, \mathbf{x}_o)$, therefore modeling the conditional densities $p_t(\boldsymbol{\theta}|\mathbf{x}_o)$ (Song et al., 2021). For example, in classifier free-guidance (Ho & Salimans, 2022), this conditioning is randomly dropped and set to 0 during training. The resulting models can then be used for both conditional and unconditional generation.

A fundamental problem here is that the conditioning \mathbf{x}_o is static, whereas we propose to have a dynamic control mechanism that depends on the trajectory $\boldsymbol{\theta}_t$, the observation, and an underlying control signal. The latter should relate $\boldsymbol{\theta}_t$ and observation using a physics-based model represented through a cost function C . As the accuracy of neural networks is inherently limited by the finite size of their weights, and smaller networks are attractive from a computational perspective, physics-based control has the potential to yield high accuracy with lean and efficient neural network models.

1-step prediction An additional issue is that the current trajectory $\boldsymbol{\theta}_t$ might not be close to a good estimate of a posterior sample $\boldsymbol{\theta}_1$, especially at the beginning of inference, where $\boldsymbol{\theta}_0$ is drawn from the sampling distribution. This issue is alleviated by applying the cost function C to the current estimate $\boldsymbol{\theta}_t$, we extrapolate $\boldsymbol{\theta}_t$ forward in time to obtain an estimated $\hat{\boldsymbol{\theta}}_1$

$$\hat{\boldsymbol{\theta}}_1 = \boldsymbol{\theta}_t + (1 - t)v_\phi(t, \boldsymbol{\theta}_t, \mathbf{x}_o). \quad (7)$$

Comparison with likelihood-guidance The 1-step prediction is conceptually related to diffusion sampling using likelihood-guidance (Chung et al., 2022; Wu et al., 2023). For inference in diffusion models, sampling is based on the conditional score $\nabla_{\theta_t} \log p(\theta_t | x_o)$, which can be decomposed into

$$\nabla_{\theta_t} \log p(\theta_t | x_o) = \nabla_{\theta_t} \log p(\theta_t) + \nabla_{\theta_t} \log p(x_o | \theta_t). \quad (8)$$

The first expression can be estimated using a pretrained diffusion model, whereas the latter is usually intractable, but can be approximated using $p(x_o | \theta_t) \approx p_{x_o | \theta_0}(x_o | \hat{\theta}(\theta_t))$, where the denoising estimate $\hat{\theta}(\theta_t) := \mathbb{E}_q[\theta_0 | \theta_t]$ is usually obtained via Tweedie’s formula $(\mathbb{E}_q[\theta_0 | \theta_t] - \theta_t)/t\sigma^2$. In practice, the estimate $\hat{\theta}(\theta_t)$ is very poor when θ_t is still noisy, impeding the inference in the early stages. On the contrary, flows based on linear conditional transportation paths have empirically been shown to have trajectories with less curvature (Lipman et al., 2023) compared to, for example, diffusion models, thus enabling inference in fewer steps and providing better estimates for $\hat{\theta}_1$.

Controlled flow v_ϕ^C We pretrain the flow network $v_\phi(t, \theta, x_o)$ without any control signals to make sure that we can realize the best achievable performance possible based on learning alone. Then, in a second training phase, we introduce the control network $v_\phi^C(t, v, c)$ with pretrained flow v and control signal c as input. The control network is much smaller in size than the flow network, making up ca. 10% of the weights ϕ in our large-scale experiments. We freeze the network weights of v_ϕ and train with the conditional flow matching loss eq. 3 for a small number of additional steps. This reduces training time and compute since we do not need to backpropagate gradients through $v_\phi(t, \theta, x_o)$. We did not observe that freezing the weights of v_ϕ affects the performance negatively. We include algorithms for training in appendix A.

4.1 TYPES OF CONTROL SIGNALS

Aiming for high inference accuracy, we extend self-conditioning via physics-based control signals to include an additional feedback loop between the model output and an underlying physics-based prior. We distinguish between two types of control signals.

Gradient-based control signal In the first case, there is a differentiable cost function C and a deterministic differentiable simulator S as shown in fig. 2a. Given an observation x_o and the estimated prediction $\hat{\theta}_1$, the control signal relates to how well $\hat{\theta}_1$ explains x_o via some cost function C . The cost function can also depend directly on or be equal to the likelihood $p(x_o | \hat{\theta}_1)$. For a differentiable cost function C , we define the control signal via

$$c(\hat{\theta}_1, x_o) := [C(S(\hat{\theta}_1), x_o); \nabla_{\hat{\theta}_1} C(S(\hat{\theta}_1), x_o)]. \quad (9)$$

Note that while we recommend using informative control signals, we can use any control that depends on $\hat{\theta}_1$ and x_o .

Learning-based control signal In the second case, the simulator is non-differentiable. To combine the simulator output with the observation x_o , we introduce a learnable encoder model Enc with parameters ϕ_E . The output of the encoder is small and of size $O(\dim(\theta))$. The control signal is then defined as

$$c(\hat{\theta}_1, x_o) := Enc(S(\hat{\theta}_1), x_o). \quad (10)$$

The gradient backpropagation is stopped at the simulator output, see fig. 2b.

4.2 ADDITIONAL CONSIDERATIONS FOR SIMULATOR FEEDBACK

Stochastic simulators Many Bayesian inference problems have a stochastic simulator. For simplicity, we assume that all stochasticity within such a simulator can be controlled via a variable

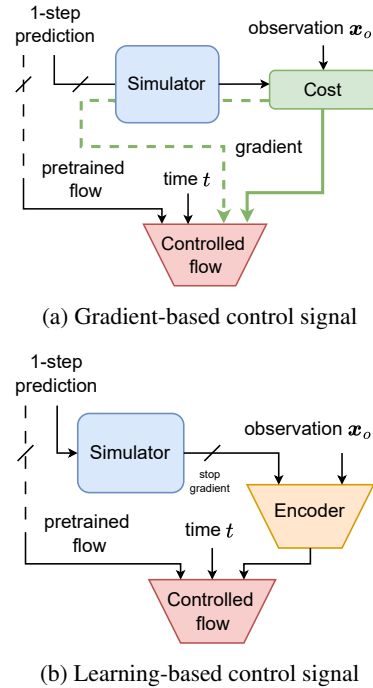


Figure 2: Control signals with simulator feedback.

$z \sim \mathcal{N}(0, I)$, which is an additional input. Motivated by the equivalence of exchanging expectation and gradient

$$\nabla_{\hat{\theta}_1} \mathbb{E}_{z \sim \mathcal{N}(0, I)} [C(S_z(\hat{\theta}_1), \mathbf{x}_o)] = \mathbb{E}_{z \sim \mathcal{N}(0, I)} [\nabla_{\hat{\theta}_1} C(S_z(\hat{\theta}_1), \mathbf{x}_o)], \quad (11)$$

when calling the simulator, we draw a random realization of z . During training, we randomly draw z for each sample and step while during inference we keep the value of z fixed for each trajectory.

Time-dependence If the estimate $\hat{\theta}_1$ is bad and the corresponding cost $C(\hat{\theta}_1, \mathbf{x}_o)$ is high, gradients and control signals can become unreliable. In appendix B, we empirically find that the estimates $\hat{\theta}_1$ become more reliable for $t \geq 0.8$. Therefore, we only train the control network v_ϕ^C in this range, which allows for focusing on control signals containing the most useful information. For $t < 0.8$, we directly output the pretrained flow $v_\phi(t, \theta, \mathbf{x}_o)$.

Theoretical correctness Contrary to likelihood-based guidance, which uses an approximation for $\nabla_{\theta_t} \log p(\mathbf{x}_o | \theta_t)$ as a guidance term during inference, the approximation $\hat{\theta}_1$ only influences the control signal, which is an input to the controlled flow network v_ϕ^C . In the case of a deterministic simulator, this makes the control signal a function of θ_t . The controlled flow network is trained with the same loss as vanilla flow matching (Lipman et al., 2023). Therefore all theoretical properties remain preserved.

5 SIMULATION-BASED INFERENCE

This section is organized as follows. First, in section 5.1, we introduce a set of SBI benchmark tasks and provide a comparison of popular neural posterior estimation (NPE) methods against a baseline of flow matching without simulator feedback. This comparison uses a similar training setup for all models and tasks. Then, in section 5.2, we focus on an optimal task-specific network with training hyperparameters based on an extensive grid search. We evaluate different variants of flow matching that are related to simulator feedback on the SBI tasks to push the performance as far as possible. In section 5.3, we pick the most challenging SBI task and improve it further by introducing simulator feedback via gradient-based and learned control signals. We carefully analyze the cost-accuracy trade-off for using simulators and show that improvements from simulator feedback cannot be replicated by increasing the training dataset size alone.

5.1 TASKS AND BASELINES

We consider the SBI tasks Lotka Volterra **LV**, a coupled ODE for the population dynamics of interacting species, **SIR**, an epidemiological model for the spread of diseases, **SLCP** and Two Moons (**TM**), two synthetic tasks having complicated multimodal posteriors. All tasks are part of the benchmark collection from Lueckmann et al. (2021). For each problem, the posterior distribution for a set of 10 observations is known, which allows for directly comparing it with the posterior predicted by the trained model. This is measured using the C2ST score (Lopez-Paz & Oquab, 2017), which trains a classifier to discriminate between samples from the true posterior and samples generated from the learned model. If the classifier cannot discriminate between two sets of samples, its test accuracy will be 0.5, whereas it increases when they become more dissimilar.

We include the following baseline methods for NPE: Continuous normalizing flows (Chen et al., 2018, CNF), Neural Spline Flows (Durkan et al., 2019, NSF), and FFJORD (Grathwohl et al., 2019). Since we propose to include feedback from simulators, here we focus on the largest benchmark budget of 10^5 simulator calls for generating the training dataset. Table 1 highlights that flow matching yields a highly competitive performance in this setting. For details on the training setup, see appendix B.

Flow matching has also been evaluated for the SBI benchmark tasks by Wildberger et al. (2023), who performed an extensive hyperparameter search for each task to find optimal hyperparameters.

Table 1: C2ST comparison with identical training setups and comparable number of network weights (ca. 300K).

Method	LV	SLCP	SIR	TM
CNF	0.99	<u>0.80</u>	0.99	0.60
NSF	0.99	-	0.75	0.54
FFJORD	<u>0.95</u>	0.82	<u>0.78</u>	0.59
<i>Flow-Mat.</i>	0.93	0.79	<u>0.79</u>	<u>0.58</u>

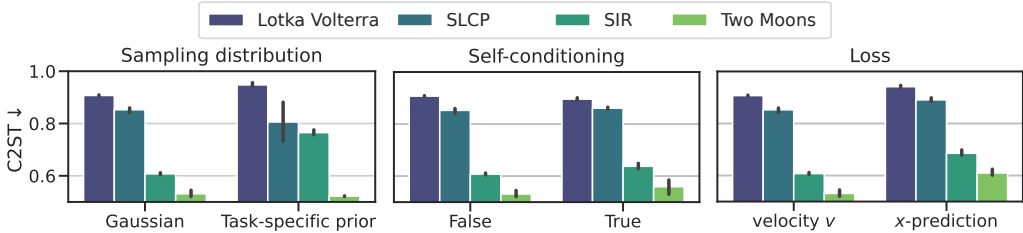


Figure 3: Evaluation of SBI tasks using different variants of flow matching training. Lower C2ST scores are better.

In the following, we focus on flow matching, and hence use the corresponding sets of optimal hyperparameters for each task.

5.2 TRAINING VARIANTS

There are several variants of training diffusion models that can be related to simulation feedback and which we consider promising in the context of SBI. Before we go on to evaluate the simulator feedback in section 5.3, we test if we can improve the performance using any of them. In particular, we assess the following modifications:

- Self-conditioning:** conditioning a model on something that depends on its own output can be seen as a form of self-conditioning. We evaluate an adapted version of self-conditioning (Chen et al., 2023). Instead of providing θ_t to the flow network, the input is comprised of the concatenated vector $[\theta_t; \text{Dropout}(\hat{\theta}_1)]$, where $\hat{\theta}_1$ is the 1-step prediction eq. 7. For computing $\hat{\theta}_1$, we require one network evaluation with the input $[\theta_t; 0]$ and stop the gradient backpropagation at $\hat{\theta}_1$. This method is similar to our simulator feedback, as it introduces a feedback loop that conditions the model on its own output, but without any simulator.
- Independent couplings:** It is also possible to couple two non-Gaussian distributions by defining the coupling as $q(z) = p_0(\theta_0)p_1(\theta_1)$ and setting the conditional probabilities to the linear paths defined by $p_t(\theta|\theta_0, \theta_1) = \mathcal{N}(\theta|t\theta_1 + (1-t)\theta_0, \sigma I)$ and $u_t(\theta|(\theta_0, \theta_1)) = \theta_1 - \theta_0$ with bandwidth $\sigma > 0$ (Liu et al., 2023; Tong et al., 2023). We can choose p_0 as the prior distribution $p(\theta)$ which we know in the SBI setting. Obtaining information in the form of an observation changes our knowledge about θ from the prior distribution to the posterior, therefore resembling a transformation similar to the noise to data transformation in diffusion models. This also suggests that the prior distribution can be closer to the posterior than a noise distribution.
- x -prediction:** The reliability of the control signal depends directly on the 1-step estimate $\hat{\theta}$. Instead of regressing the flow $u_t(\theta)$, we can directly predict the denoised estimate $\hat{\theta}$ and obtain the velocity by rearranging eq. 7, giving $v_\phi(t, \theta_t, \mathbf{x}_o) = \hat{\theta}_1/(1-t)$. We additionally weight the x -prediction loss with a time-dependent weighting $w_t := 1/(1-t)$ to account for the scaling in eq. 7. The x -prediction potentially produces better estimates for $\hat{\theta}$, thus allowing for obtaining more reliable feedback from control signals when $t < 0.8$.

Evaluation Figure 3 shows an evaluation of the different variants against vanilla flow matching (Gaussian sampling distribution, no self-conditioning and velocity prediction). Using task-specific priors produces outliers with better C2ST scores for SLCP but is consistently worse for LV and SIR. We conclude that normal Gaussian distributions are more suited as sampling distributions for most low-dimensional problems. Introducing self-conditioning does not show any improvements, so feedback loops without a simulator alone are not sufficient for better performance in this situation. Finally, the x -prediction loss consistently performs worse than the velocity prediction. Therefore, a potential improvement in the 1-step estimate is outweighed by a corresponding deterioration of the posterior correctness as indicated by the C2ST score.

5.3 SIMULATOR FEEDBACK: GRADIENT-BASED AND LEARNED

In this section, we focus on the Lotka-Volterra (LV) task for a more detailed analysis. It has the highest difficulty as seen by the C2ST score, and we use it to test the different types of feedback. We reimplement the LV simulator in JAX (Bradbury et al., 2018) to support differentiability and evaluate the gradient-based control signal as well as the learning-based control signal, using a small multilayer perceptron (MLP). In addition, to make sure that observed improvements are not due to the increased number of network parameters and finetuning with the control network, we also evaluate a variant where we finetune with the control network but set all simulator-dependent inputs to the control network to 0 (Zero Controls). We show an evaluation with C2ST in fig. 4. For both the learning and gradient-based control signals we see clear improvements with the gradient-based signal clearly ahead. The zero control signal improves only slightly, showing that the improvement can be directly attributed to the simulator. While control signals are most useful for more high-dimensional problems with less sparse and noisy observations, this experiment demonstrates that they can also be used in low-dimensional settings. Moreover, while differentiable simulators can provide better control signals, feedback from non-differentiable simulators likewise shows clear improvements.

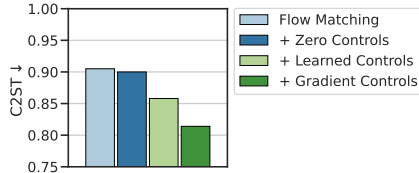


Figure 4: Evaluation of simulator feedback for LV.

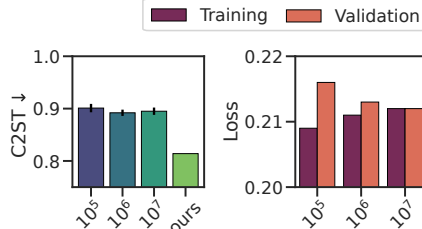


Figure 5: Different simulator call budgets (training set sizes 10^5 , 10^6 , 10^7) compared with finetuning using simulator feedback (ours, ca. 9×10^6 simulator calls in total).

5.4 COMPUTATIONAL EFFICIENCY

A critical issue in SBI is that calls to the simulator are potentially expensive. This imposes the question of whether compute time is better spent on extending the training dataset or training with feedback from the simulator. We empirically verify that the latter is more efficient for the LV task in this setup by comparing our method to models with an increased training dataset from a larger simulator budget. Specifically, we train with dataset sizes of 10^6 and 10^7 . Training the gradient-based control signal took ca. 9×10^6 simulator calls. See fig. 5 for the evaluation. There is no improvement in the C2ST for models trained without simulator feedback beyond 10^5 data points, and the final train/validation loss for the 10^7 model indicates that there is no more overfitting. Nonetheless, the model trained with controls clearly outperforms the model trained with more data, indicating that the directed feedback of the simulator cannot be replaced by increased amounts of training data.

6 STRONG GRAVITATIONAL LENSING

We present our results for modeling strong gravitational lens systems, a challenging and highly relevant non-linear problem in astronomy. Strong gravitational lensing is a physical phenomenon whereby the light rays by a distant object, such as a galaxy, are deflected by an intervening massive object, such as another galaxy or a galaxy cluster. As a result, one observes multiple distorted images of the background source. We aim to recover both the lens and source light distribution as well as the lens mass density distribution with realistic simulated observations for which we know the ground truths. We evaluate flow matching as an NPE method with gradient-based control signals from a differentiable simulator with two MCMC methods.

Lens modeling The *lens equation* relates coordinates on the source plane β and the observed image plane Θ via the deflection angle α induced by the mass profile or gravitational potential of the lens galaxy. We use a Singular Isothermal Ellipsoid (SIE) to describe this lens mass and Sérsic profiles for both the source light and light emitted from the lens galaxy (full details are provided in appendix C). There are 9 parameters for the lens mass and 7 parameters for each Sérsic profile, giving 23 parameters in total. The likelihood is measured by the χ^2 -statistic, which is the modeled image plane Θ minus the observation x_o divided by the noise. To solve the lensing equation, we make use of

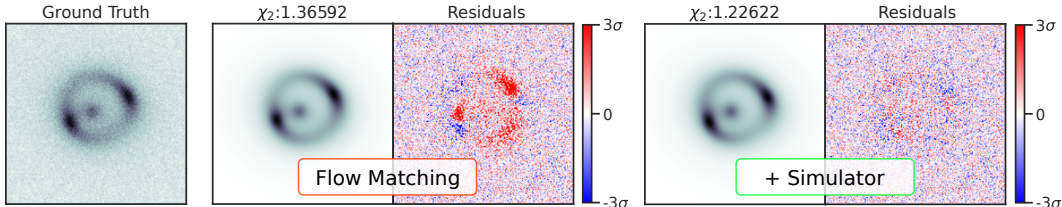


Figure 6: Reconstruction of observation. Flow matching is purely learning-based and shows noticeable residuals in the reconstruction. Including simulator feedback removes remaining residuals.

the publicly available raytracing code by (Galan et al., 2022). We want to stress that even small perturbations of the model parameters can cause the χ_2 to increase significantly; see fig. 13 in the appendix.

Datasets and pretraining Several instrument-specific measurement effects are included when simulating the observations. We include background and Poisson noise and smoothing by a point-spread function (PSF). The pixel size corresponds to 0.04 arc seconds. These directly affect the posterior, as more noise and a stronger PSF will widen the posterior distribution. We generate 250 000 data samples for training and 25 000 for validation. The flow network v_ϕ consists of a convolutional feature extraction neural network represented by a shallow CNN whose output is fed into a dense feed-forward neural network with residual blocks. Full details are in appendix C.

Finetuning with control signals The control network v_ϕ^C is represented by another dense feed-forward network, which accounts for 11% of all parameters in the combined model. The control signals are obtained from simulating an observation based on the predicted estimate $\hat{\theta}_1$ via ray-tracing (Galan et al., 2022) based on the parametric models, calculating the χ_2 -statistic and computing gradients with respect to the estimate θ_1 . The χ_2 -statistic itself is also part of the control signal.

Reference posteriors As reference posteriors, we include Hamiltonian Monte Carlo (HMC) with No-U-Turn sampler (Hoffman et al., 2014, NUTS) and Affine-Invariant Ensemble Sampling (Goodman & Weare, 2010, AIES), which are both two popular MCMC-methods in astronomy. We adopt implementations of both methods using numpyro (Phan et al., 2019; Bingham et al., 2019). Details on running both methods can be found in appendix C. Additionally, we compare to diffusion posterior sampling as a learned baseline (Chung et al., 2023b, DPS), see appendix C.1 for details. We use Euler integration for both flow matching variants.

6.1 EVALUATION AND DISCUSSION

χ_2 -statistic We show an evaluation of all methods in table 2. The average χ_2 is computed over 1000 randomly chosen validation systems, where for each, we draw 1000 samples from the posterior. If we compute the χ_2 for the ground truth parameters, we obtain a value of 1.17 due to the noise in the observation. Since we cannot overfit to noise with the parametric models, this represents a lower bound for χ_2 in this experiment. Including the physics-based control improves the χ_2 from 1.83 to 1.48, representing an improvement of 53% relative to the best modeling. The improved χ_2 is even better than the best baseline method, AIES.

Table 2: Evaluation with respect to average χ_2 and inference time for the posterior distribution.

Method	Avg. $\chi_2 \downarrow$	Modeling Time \downarrow
NUTS	1.83	$\sim 56x$ (564s)
AIES	1.74	$\sim 67x$ (672s)
DPS	9.98	$\sim 42x$ (427s)
<i>Flow-Mat.</i>	1.83	1x (10s)
+ Simulator	1.48	$\sim 2x$ (19s)

Modeling time We define the modeling time as the average compute time required to produce 1000 credible posterior samples. Both HMC and AIES require significant warmup times before producing the first samples from the posterior, which we include in the table. However, after warmup, it is relatively cheap to obtain new samples. On the other hand, flow matching does not require any warmup time and the modeling time increases linearly with the number of posterior samples.

All methods were implemented in JAX (Bradbury et al., 2018) and used the same hardware. The measurements in table 2 show that DPS is faster than the classic baselines, but yields a very sub-optimal performance in terms of its distribution. The performance numbers also highlight that our method yields an accuracy that surpasses AIES, while being more than 30x faster. This evaluation demonstrates that flow matching-based methods are highly competitive even in small to moderate-sized problems where established MCMC methods in terms of accuracy exist, clearly beating them in terms of inference time. Flow matching with our proposed control signals is especially interesting because it is not affected as much by the curse of dimensionality as traditional inference methods and allows for having non-trivial learnable high-dimensional priors. However, before these methods are widely trusted, they need to demonstrate their competitiveness with classical methods. Our results show that this is indeed the case, which opens up exciting avenues for applying and developing approaches targeting similar and adjacent inverse problems in science.

Simulation-based calibration Acquiring truthful posterior distributions for Bayesian inference problems is difficult, which makes it hard to robustly evaluate whether the predicted posterior distribution is correct. We use simulation-based calibration (Talts et al., 2018, SBC) as an additional evaluation tool. The data-averaged posterior obtained from averaging the posterior distribution over many problem instances has to be equal to the prior. This can be tested by considering a one-dimensional function $f : \theta \mapsto \mathbb{R}$ and L samples $\theta^1, \dots, \theta^L$ drawn from an inference method. If θ^* are the ground truth parameters, then the rank statistic $\sum_{l=1}^L \mathbf{1}_{f(\theta^l) < f(\theta^*)}$ has to be uniformly distributed over the integers $[0, L]$. If the distribution of the rank statistic is plotted as a histogram, systematic problems in the inference method can be identified visually, see fig. 7. We set $L = 1000$ and plot the histograms for all $n = 1000$ test problems and visualize the parameter x_{center} , which defines the position of the source in x -direction. The posteriors without simulator feedback are biased, as can be seen in the deviation from uniformity in the plots. Including simulator feedback improves the distribution of the rank statistic. For an extended analysis, see appendix C.2.

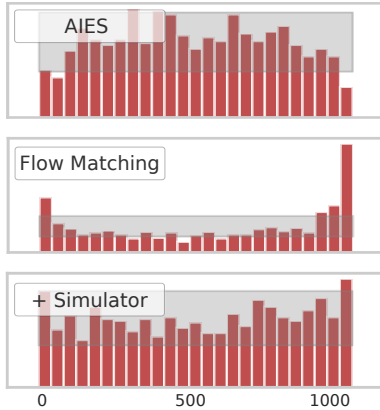


Figure 7: SBC for x_{center} of the source galaxy.

6.2 LIMITATIONS

While introducing additional control signals increases the quality of produced samples, it comes at the cost of slower inference and training times depending on the speed of the simulator. In general, using non-differentiable control signals is possible but removes the possibility of computing likelihoods via the instantaneous change of variables formula (Chen et al., 2018). Compared to MCMC approaches, inference with flow-based models requires a substantial upfront cost for training that needs to be amortized across many problems. Additionally, priors are encoded in the learned flow networks, so changing them would require retraining models with adjusted data sets.

7 CONCLUSION

We presented a method for improving flow-based models with simulator feedback using control signals. This allows us to refine an existing flow with only a few additional weights and little training time. We thereby efficiently bridge the gap between purely learning-based methods for simulation-based inference and optimization with hand-crafted cost functions within the framework of flow matching. This improvement is critical for scientific applications where high accuracy and trustworthiness in the methods are required. Purely learning-based methods face significant difficulties in producing very accurate samples, as there is usually no feedback during inference of how good samples are. In this paper, we demonstrated that we do not need large network sizes or tremendous amounts of data to train accurate models that are competitive with established MCMC methods if we include suitable control signals from simulators. We believe this work makes an important step towards making posterior inference in science more accurate, understandable, and reliable.

REFERENCES

- Michael S. Albergo, Nicholas M. Boffi, and Eric Vanden-Eijnden. Stochastic interpolants: A unifying framework for flows and diffusions. *CoRR*, abs/2303.08797, 2023a. doi: 10.48550/ARXIV.2303.08797. URL <https://doi.org/10.48550/arXiv.2303.08797>.
- Michael S. Albergo, Mark Goldstein, Nicholas M. Boffi, Rajesh Ranganath, and Eric Vanden-Eijnden. Stochastic interpolants with data-dependent couplings. *CoRR*, abs/2310.03725, 2023b. doi: 10.48550/ARXIV.2310.03725. URL <https://doi.org/10.48550/arXiv.2310.03725>.
- Atilim Gunes Baydin, Lei Shao, Wahid Bhimji, Lukas Heinrich, Saeid Naderiparizi, Andreas Munk, Jialin Liu, Bradley Gram-Hansen, Gilles Louppe, Lawrence Meadows, Philip H. S. Torr, Victor W. Lee, Kyle Cranmer, Prabhat, and Frank Wood. Efficient probabilistic inference in the quest for physics beyond the standard model. In *Advances in Neural Information Processing Systems 32*, pp. 5460–5473, 2019. URL <https://proceedings.neurips.cc/paper/2019/hash/6d19c113404cee55b4036fcela37c058-Abstract.html>.
- Eli Bingham, Jonathan P. Chen, Martin Jankowiak, Fritz Obermeyer, Neeraj Pradhan, Theofanis Karaletsos, Rohit Singh, Paul A. Szerlip, Paul Horsfall, and Noah D. Goodman. Pyro: Deep universal probabilistic programming. *J. Mach. Learn. Res.*, 20:28:1–28:6, 2019. URL <http://jmlr.org/papers/v20/18-403.html>.
- James Bradbury, Roy Frostig, Peter Hawkins, Matthew James Johnson, Chris Leary, Dougal Maclaurin, George Necula, Adam Paszke, Jake VanderPlas, Skye Wanderman-Milne, and Qiao Zhang. JAX: composable transformations of Python+NumPy programs, 2018. URL <http://github.com/google/jax>.
- Gabriel Cardoso, Yazid Janati El Idrissi, Sylvain Le Corff, and Eric Moulines. Monte carlo guided diffusion for bayesian linear inverse problems. *CoRR*, abs/2308.07983, 2023. doi: 10.48550/ARXIV.2308.07983. URL <https://doi.org/10.48550/arXiv.2308.07983>.
- Tian Qi Chen, Yulia Rubanova, Jesse Bettencourt, and David Duvenaud. Neural ordinary differential equations. In *Advances in Neural Information Processing Systems 31*, pp. 6572–6583, 2018. URL <https://proceedings.neurips.cc/paper/2018/hash/69386f6bb1dfed68692a24c8686939b9-Abstract.html>.
- Ting Chen, Ruixiang Zhang, and Geoffrey E. Hinton. Analog bits: Generating discrete data using diffusion models with self-conditioning. In *The Eleventh International Conference on Learning Representations, ICLR 2023, Kigali, Rwanda, May 1-5, 2023*. OpenReview.net, 2023. URL <https://openreview.net/pdf?id=3itjR9QxFw>.
- Hyungjin Chung, Byeongsu Sim, and Jong Chul Ye. Come-closer-diffuse-faster: Accelerating conditional diffusion models for inverse problems through stochastic contraction. In *IEEE/CVF Conference on Computer Vision and Pattern Recognition, CVPR 2022, New Orleans, LA, USA, June 18-24, 2022*, pp. 12403–12412. IEEE, 2022. doi: 10.1109/CVPR52688.2022.01209. URL <https://doi.org/10.1109/CVPR52688.2022.01209>.
- Hyungjin Chung, Jeongsol Kim, Michael Thompson McCann, Marc Louis Klasky, and Jong Chul Ye. Diffusion posterior sampling for general noisy inverse problems. In *The Eleventh International Conference on Learning Representations, ICLR 2023, Kigali, Rwanda, May 1-5, 2023*. OpenReview.net, 2023a. URL <https://openreview.net/pdf?id=OnD9zGAGT0k>.
- Hyungjin Chung, Jeongsol Kim, and Jong Chul Ye. Direct diffusion bridge using data consistency for inverse problems. In *Advances in Neural Information Processing Systems 36*, 2023b. URL http://papers.nips.cc/paper_files/paper/2023/hash/165b0e600b1721bd59526131eb061092-Abstract-Conference.html.
- Kyle Cranmer, Johann Brehmer, and Gilles Louppe. The frontier of simulation-based inference. *Proceedings of the National Academy of Sciences*, 117(48):30055–30062, 2020.
- Pedro VP Cunha and Carlos AR Herdeiro. Shadows and strong gravitational lensing: a brief review. *General Relativity and Gravitation*, 50:1–27, 2018.

- Maximilian Dax, Stephen R Green, Jonathan Gair, Jakob H Macke, Alessandra Buonanno, and Bernhard Schölkopf. Real-time gravitational wave science with neural posterior estimation. *Physical review letters*, 127(24):241103, 2021.
- Laurent Dinh, Jascha Sohl-Dickstein, and Samy Bengio. Density estimation using real NVP. In *5th International Conference on Learning Representations, ICLR 2017, Toulon, France, April 24-26, 2017, Conference Track Proceedings*. OpenReview.net, 2017. URL <https://openreview.net/forum?id=HkpbmH9lx>.
- Conor Durkan, Artur Bekasov, Iain Murray, and George Papamakarios. Neural spline flows. In *Advances in Neural Information Processing Systems 32*, pp. 7509–7520, 2019. URL <https://proceedings.neurips.cc/paper/2019/hash/7ac71d433f282034e088473244df8c02-Abstract.html>.
- A. Galan, G. Vernardos, A. Peel, F. Courbin, and J. L. Starck. Using wavelets to capture deviations from smoothness in galaxy-scale strong lenses. *Astronomy and Astrophysics*, 668:A155, December 2022. doi: 10.1051/0004-6361/202244464.
- Tilmann Gneiting and Adrian E Raftery. Weather forecasting with ensemble methods. *Science*, 310(5746):248–249, 2005.
- Jonathan Goodman and Jonathan Weare. Ensemble samplers with affine invariance. *Communications in applied mathematics and computational science*, 5(1):65–80, 2010.
- Will Grathwohl, Ricky T. Q. Chen, Jesse Bettencourt, Ilya Sutskever, and David Duvenaud. FFIORD: free-form continuous dynamics for scalable reversible generative models. In *7th International Conference on Learning Representations, ICLR 2019, New Orleans, LA, USA, May 6-9, 2019*. OpenReview.net, 2019. URL <https://openreview.net/forum?id=rJxgknCcK7>.
- Arthur Gretton, Karsten M Borgwardt, Malte J Rasch, Bernhard Schölkopf, and Alexander Smola. A kernel two-sample test. *The Journal of Machine Learning Research*, 13(1):723–773, 2012.
- Yashar D Hezaveh, Laurence Perreault Lévassieur, and Philip J Marshall. Fast automated analysis of strong gravitational lenses with convolutional neural networks. *Nature*, 548(7669):555–557, 2017.
- Jonathan Ho and Tim Salimans. Classifier-free diffusion guidance. *CoRR*, abs/2207.12598, 2022. doi: 10.48550/ARXIV.2207.12598. URL <https://doi.org/10.48550/arXiv.2207.12598>.
- Jonathan Ho, Ajay Jain, and Pieter Abbeel. Denoising diffusion probabilistic models. In *Advances in Neural Information Processing Systems 33*, 2020. URL <https://proceedings.neurips.cc/paper/2020/hash/4c5bcfec8584af0d967f1ab10179ca4b-Abstract.html>.
- Matthew D Hoffman, Andrew Gelman, et al. The no-u-turn sampler: adaptively setting path lengths in hamiltonian monte carlo. *J. Mach. Learn. Res.*, 15(1):1593–1623, 2014.
- Benjamin J. Holzschuh, Simona Vegetti, and Nils Thuerey. Solving inverse physics problems with score matching. In *Advances in Neural Information Processing Systems 36*, 2023. URL http://papers.nips.cc/paper_files/paper/2023/hash/c2f2230abc7ccf669f403be881d3ffb7-Abstract-Conference.html.
- Bahjat Kawar, Gregory Vaksman, and Michael Elad. SNIPS: solving noisy inverse problems stochastically. In *Advances in Neural Information Processing Systems 34*, pp. 21757–21769, 2021. URL <https://proceedings.neurips.cc/paper/2021/hash/b5c01503041b70d41d80e3dbe31bbd8c-Abstract.html>.
- Bahjat Kawar, Michael Elad, Stefano Ermon, and Jiaming Song. Denoising diffusion restoration models. In *Advances in Neural Information Processing Systems 35*, 2022. URL http://papers.nips.cc/paper_files/paper/2022/hash/95504595b6169131b6ed6cd72eb05616-Abstract-Conference.html.

- Diederik P. Kingma and Jimmy Ba. Adam: A method for stochastic optimization. In Yoshua Bengio and Yann LeCun (eds.), *3rd International Conference on Learning Representations, ICLR 2015, San Diego, CA, USA, May 7-9, 2015, Conference Track Proceedings*, 2015. URL <http://arxiv.org/abs/1412.6980>.
- Diederik P. Kingma and Prafulla Dhariwal. Glow: Generative flow with invertible 1x1 convolutions. In *Advances in Neural Information Processing Systems 31*, pp. 10236–10245, 2018. URL <https://proceedings.neurips.cc/paper/2018/hash/d139db6a236200b21cc7f752979132d0-Abstract.html>.
- Rene Laureijs, J Amiaux, S Arduini, J-L Augueres, J Brinchmann, R Cole, M Cropper, C Dabin, L Duvet, A Ealet, et al. Euclid definition study report. *arXiv preprint arXiv:1110.3193*, 2011.
- Ronan Legin, Yashar Hezaveh, Laurence Perreault Lévassieur, and Benjamin Wandelt. Simulation-based inference of strong gravitational lensing parameters. *arXiv preprint arXiv:2112.05278*, 2021.
- Ronan Legin, Yashar Hezaveh, Laurence Perreault-Lévassieur, and Benjamin Wandelt. A framework for obtaining accurate posteriors of strong gravitational lensing parameters with flexible priors and implicit likelihoods using density estimation. *The Astrophysical Journal*, 943(1):4, 2023.
- Laurence Perreault Lévassieur, Yashar D Hezaveh, and Risa H Wechsler. Uncertainties in parameters estimated with neural networks: Application to strong gravitational lensing. *The Astrophysical Journal Letters*, 850(1):L7, 2017.
- Yaron Lipman, Ricky T. Q. Chen, Heli Ben-Hamu, Maximilian Nickel, and Matthew Le. Flow matching for generative modeling. In *The Eleventh International Conference on Learning Representations, ICLR 2023, Kigali, Rwanda, May 1-5, 2023*. OpenReview.net, 2023. URL <https://openreview.net/pdf?id=PqvMRDCJT9t>.
- Xingchao Liu, Chengyue Gong, and Qiang Liu. Flow straight and fast: Learning to generate and transfer data with rectified flow. In *The Eleventh International Conference on Learning Representations, ICLR 2023, Kigali, Rwanda, May 1-5, 2023*. OpenReview.net, 2023. URL <https://openreview.net/pdf?id=XVjTT1nw5z>.
- David Lopez-Paz and Maxime Oquab. Revisiting classifier two-sample tests. In *5th International Conference on Learning Representations, ICLR 2017, Toulon, France, April 24-26, 2017, Conference Track Proceedings*. OpenReview.net, 2017. URL <https://openreview.net/forum?id=SJkXfE5xx>.
- Jan-Matthis Lueckmann, Jan Boelts, David S. Greenberg, Pedro J. Gonçalves, and Jakob H. Macke. Benchmarking simulation-based inference. In *The 24th International Conference on Artificial Intelligence and Statistics, AISTATS 2021, April 13-15, 2021, Virtual Event*, volume 130 of *Proceedings of Machine Learning Research*, pp. 343–351. PMLR, 2021. URL <http://proceedings.mlr.press/v130/lueckmann21a.html>.
- George Papamakarios, Iain Murray, and Theo Pavlakou. Masked autoregressive flow for density estimation. In *Advances in Neural Information Processing Systems 30*, pp. 2338–2347, 2017. URL <https://proceedings.neurips.cc/paper/2017/hash/6c1da886822c67822bcf3679d04369fa-Abstract.html>.
- George Papamakarios, David C. Sterratt, and Iain Murray. Sequential neural likelihood: Fast likelihood-free inference with autoregressive flows. In Kamalika Chaudhuri and Masashi Sugiyama (eds.), *The 22nd International Conference on Artificial Intelligence and Statistics, AISTATS*, volume 89 of *Proceedings of Machine Learning Research*, pp. 837–848. PMLR, 2019. URL <http://proceedings.mlr.press/v89/papamakarios19a.html>.
- Du Phan, Neeraj Pradhan, and Martin Jankowiak. Composable effects for flexible and accelerated probabilistic programming in numpyro. *arXiv preprint arXiv:1912.11554*, 2019.
- Jason Poh, Ashwin Samudre, Aleksandra Ćiprijanović, Brian Nord, Gourav Khullar, Dimitrios Tanoglidis, and Joshua A Frieman. Strong lensing parameter estimation on ground-based imaging data using simulation-based inference. *arXiv preprint arXiv:2211.05836*, 2022.

- Aram-Alexandre Pooladian, Heli Ben-Hamu, Carles Domingo-Enrich, Brandon Amos, Yaron Lipman, and Ricky T. Q. Chen. Multisample flow matching: Straightening flows with minibatch couplings. In Andreas Krause, Emma Brunskill, Kyunghyun Cho, Barbara Engelhardt, Sivan Sabato, and Jonathan Scarlett (eds.), *International Conference on Machine Learning, ICML 2023, 23-29 July 2023, Honolulu, Hawaii, USA*, volume 202 of *Proceedings of Machine Learning Research*, pp. 28100–28127. PMLR, 2023. URL <https://proceedings.mlr.press/v202/pooladian23a.html>.
- Danilo Jimenez Rezende and Shakir Mohamed. Variational inference with normalizing flows. In *Proceedings of the 32nd International Conference on Machine Learning, ICML 2015, Lille, France, 6-11 July 2015*, volume 37 of *JMLR Workshop and Conference Proceedings*, pp. 1530–1538. JMLR.org, 2015. URL <http://proceedings.mlr.press/v37/rezende15.html>.
- Chitwan Saharia, William Chan, Saurabh Saxena, Lala Li, Jay Whang, Emily L. Denton, Seyed Kamyar Seyed Ghasemipour, Raphael Gontijo Lopes, Burcu Karagol Ayan, Tim Salimans, Jonathan Ho, David J. Fleet, and Mohammad Norouzi. Photorealistic text-to-image diffusion models with deep language understanding. In *Advances in Neural Information Processing Systems 35*, 2022. URL http://papers.nips.cc/paper_files/paper/2022/hash/ec795aeadae0b7d230fa35cbaf04c041-Abstract-Conference.html.
- S Schuldt, SH Suyu, T Meinhardt, L Leal-Taixé, R Cañameras, S Taubenberger, and A Halkola. Holismokes-iv. efficient mass modeling of strong lenses through deep learning. *Astronomy & Astrophysics*, 646:A126, 2021.
- Louis Sharrock, Jack Simons, Song Liu, and Mark Beaumont. Sequential neural score estimation: Likelihood-free inference with conditional score based diffusion models. *CoRR*, abs/2210.04872, 2022. doi: 10.48550/ARXIV.2210.04872. URL <https://doi.org/10.48550/arXiv.2210.04872>.
- Yang Song, Jascha Sohl-Dickstein, Diederik P. Kingma, Abhishek Kumar, Stefano Ermon, and Ben Poole. Score-based generative modeling through stochastic differential equations. In *9th International Conference on Learning Representations, ICLR 2021, Virtual Event, Austria, May 3-7, 2021*. OpenReview.net, 2021. URL <https://openreview.net/forum?id=PxtIG12RRHS>.
- Sean Talts, Michael Betancourt, Daniel Simpson, Aki Vehtari, and Andrew Gelman. Validating bayesian inference algorithms with simulation-based calibration. *arXiv preprint arXiv:1804.06788*, 2018.
- Alexander Tong, Nikolay Malkin, Guillaume Hugué, Yanlei Zhang, Jarrid Rector-Brooks, Kilian Fatras, Guy Wolf, and Yoshua Bengio. Conditional flow matching: Simulation-free dynamic optimal transport. *CoRR*, abs/2302.00482, 2023. doi: 10.48550/ARXIV.2302.00482. URL <https://doi.org/10.48550/arXiv.2302.00482>.
- S Vegetti, S Birrer, G Despali, CD Fassnacht, D Gilman, Y Hezaveh, L Perreault Levasseur, JP McKean, DM Powell, CM O’Riordan, et al. Strong gravitational lensing as a probe of dark matter. *arXiv preprint arXiv:2306.11781*, 2023.
- Simona Vegetti and Léon VE Koopmans. Bayesian strong gravitational-lens modelling on adaptive grids: objective detection of mass substructure in galaxies. *Monthly Notices of the Royal Astronomical Society*, 392(3):945–963, 2009.
- Jonas Wildberger, Maximilian Dax, Simon Buchholz, Stephen R. Green, Jakob H. Macke, and Bernhard Schölkopf. Flow matching for scalable simulation-based inference. In *Advances in Neural Information Processing Systems 36*, 2023. URL http://papers.nips.cc/paper_files/paper/2023/hash/3663ae53ec078860bb0b9c6606e092a0-Abstract-Conference.html.
- Luhuan Wu, Brian L. Trippe, Christian A. Naesseth, David M. Blei, and John P. Cunningham. Practical and asymptotically exact conditional sampling in diffusion models. In *Advances in Neural Information Processing Systems 36*, 2023. URL http://papers.nips.cc/paper_files/paper/2023/hash/63e8bc7bbf1cfea36d1db6538aecce5-Abstract-Conference.html.

APPENDIX

A ALGORITHMS

We include algorithms for training using flow matching and control signals, see algorithm 1. For flow matching with self-conditioning, see algorithm 2.

Algorithm 1 FM with Control Signals

Input: Training distribution q_1 , pretrained network v_ϕ , control network v_ϕ^C , σ_{\min}

while Training **do**

$(\theta_1, \mathbf{x}_o) \sim q_1; z \leftarrow \mathcal{N}(0, I)$

$\theta \leftarrow t\theta_1 + (1-t)z$

$\mathbf{v} \leftarrow \text{stopgrad}(v_\phi(t, \theta, \mathbf{x}_o))$

$\hat{\theta}_1 \leftarrow \theta + (1-t)\mathbf{v}$

$\mathbf{c} \leftarrow \text{control}(\hat{\theta}_1, \mathbf{x}_o)$

$\tilde{\mathbf{v}} \leftarrow v_\phi^C(t, \mathbf{v}, \mathbf{c}) + \mathbf{v}$

$u_t(\theta|\theta_1, \mathbf{x}_o) \leftarrow \frac{\theta_1 - (1 - \sigma_{\min})\theta}{1 - (1 - \sigma_{\min})t}$

$\mathcal{L}_{\text{CFM}} \leftarrow \|\tilde{\mathbf{v}} - u_t(\theta|\theta_1, \mathbf{x}_o)\|_2^2$

$\theta \leftarrow \text{Update}(\phi, \nabla_\phi \mathcal{L}_{\text{CFM}}(\phi))$

return: v_ϕ, v_ϕ^C

Algorithm 2 FM with Self-conditioning

Input: Training distribution q_1 , flow network v_ϕ, σ_{\min}

while Training **do**

$(\theta_1, \mathbf{x}_o) \sim q_1; z \leftarrow \mathcal{N}(0, I); s \leftarrow \mathcal{U}(0, 1)$

$\theta \leftarrow t\theta_1 + (1-t)z; \hat{\theta}_1 \leftarrow 0$

$\mathbf{v} \leftarrow \text{stopgrad}(v_\theta(t, [\theta, \hat{\theta}_1], \mathbf{x}_o))$

if $s > 0.5$ **then**

$\hat{\theta}_1 \leftarrow \theta + (1-t)\mathbf{v}$

$\tilde{\mathbf{v}} \leftarrow v_\phi(t, [\theta, \hat{\theta}_1], \mathbf{x}_o)$

$u_t(\theta|\theta_1, \mathbf{x}_o) \leftarrow \frac{\theta_1 - (1 - \sigma_{\min})\theta}{1 - (1 - \sigma_{\min})t}$

$\mathcal{L}_{\text{CFM}} \leftarrow \|\tilde{\mathbf{v}} - u_t(\theta|\theta_1, \mathbf{x}_o)\|_2^2$

$\theta \leftarrow \text{Update}(\phi, \nabla_\phi \mathcal{L}_{\text{CFM}}(\phi))$

return: v_ϕ

B SIMULATION-BASED INFERENCE

Baselines comparison in section 5.1 For a fairer comparison, we set up all baseline methods with a similar number of network weights and available compute time.

We train all baselines and flow matching with a batch size of 512 on the largest 10^5 simulation budgets for all tasks. For optimization, we apply Adam (Kingma & Ba, 2015) with default settings and constant learning rate of 10^{-4} and weight decay 2×10^{-5} .

All network architectures are chosen to have a similar number of ca. $3 \cdot 10^5$ parameters. For flow matching and continuous normalizing flows (CNFs), we use the same architecture based on a dense feed-forward neural net with skip connections using 8 residual blocks with each 128 neurons and *elu* activation. As input, we concatenate time t and θ_t . For Neural Spline Flow (Durkan et al., 2019) and FFJORD (Grathwohl et al., 2019), we adopt the released implementation by the authors.

Depending on the time per epoch for each method, we modify the number of epochs and steps per epoch to allow all methods to train for a similar amount of time, ensuring a sufficient window for convergence. For NSF, we train for 1 000 epochs, for flow matching for 2 000 epochs, and for FFJORD and CNF 100 epochs.

Flow matching with optimized hyperparameters For the experiments in section 5.2 and section 5.3, we adopt the hyperparameters and network architecture from Wildberger et al. (2023), which is based on a hyperparameter grid search. The hyperparameters for each task are listed in table 3. Otherwise, we follow the implementation as provided by the authors.

Table 3: Hyperparameters for SBI from Wildberger et al. (2023).

Task	Time α	Batch size	Learning rate	Residual blocks
LV	1	32	10^{-3}	[32, 64, 128, 256, 5×512 , 256, 128, 64, 32]
SLCP	-0.5	256	$5 \cdot 10^{-4}$	[32, 64, 128, 256, 5×512 , 256, 128, 64, 32]
SIR	4	256	$5 \cdot 10^{-4}$	[32, 64, 128, 256, 7×512 , 256, 128, 64, 32]
TM	4	64	$2 \cdot 10^{-4}$	[32, 64, 128, 256, 512, 3×1024 , 512, 128, 64, 32]

Analyzing the 1-step estimate We simulate the flow ODE from the sampling distribution at $t = 0$ until t^* (x -axis). Then, we compute the posterior in a single step by linearly extrapolating the flow, see eq. 7, to obtain the estimate $\hat{\theta}_1$. Results are shown in fig. 8.

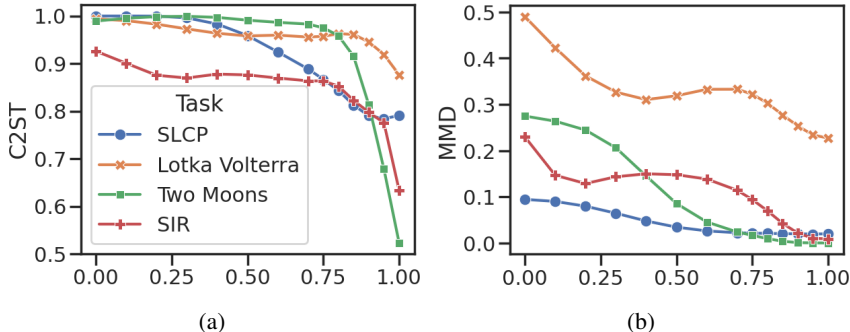


Figure 8: (a) and (b): C2ST score and MMD for predictive samples $\hat{\theta}_1$. The x -axis shows from which we compute the predictive sample.

Analyzing step size We analyze the influence of the step size of the ODE solver on the quality of the posterior distribution as shown in fig. 9.

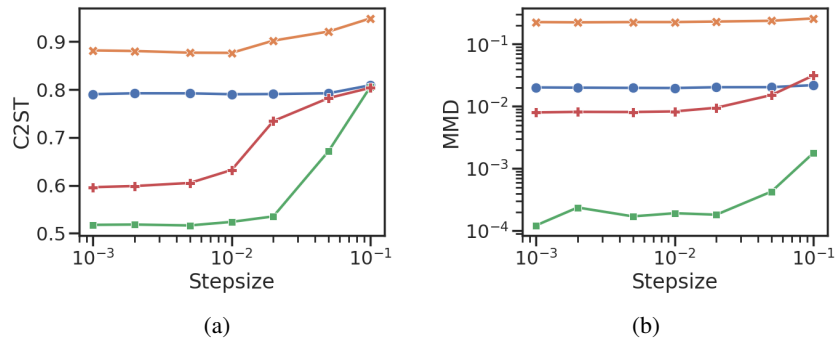


Figure 9: (a) and (b): C2ST score and MMD vs. step size during inference.

Additional results for maximum mean discrepancy For the evaluation in section 5.2, we show additional results for the maximum mean discrepancy (Gretton et al., 2012, MMD) in fig. 10.

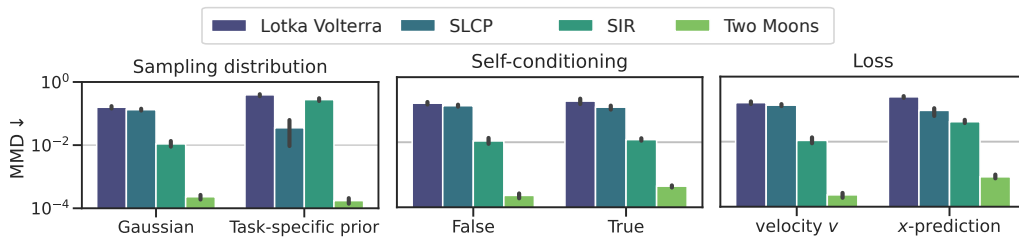


Figure 10: Evaluation of SBI tasks using different variants of flow matching training. Lower MMD scores are better.

C STRONG GRAVITATIONAL LENSING

We consider the following models:

- For modeling the lens we use an SIE model with 6 parameters: the Einstein radius θ_E , the ellipticities e_1 and e_2 and x_{center} and y_{center} . There is shear, for which we only consider γ_1 and γ_2 as free parameters.
- The source is modeled by a Sersic profile with free parameters being the amplitude, the half-light radius, the Sersic index n , the ellipticities e_1 and e_2 as well as the positions x_{center} and y_{center} .
- The lens light is modeled in the same way as the source, although when generating the mock data, we fix the position as well as ellipticities to be the same as the lens mass model. For training and inference, we infer positions for both lens mass and lens light model, so the model could produce different values for them. The MCMC methods use the same parameter for both lens light and lens mass position.

We list all priors in table 4, table 5 and table 6. We do not have priors on the ellipticities e_1 and e_2 directly, but we obtain them from priors on the position angle and axis ratio. Also, we obtain the shear parameters from γ_1 and γ_2 from ϕ_{ext} and γ_{ext} by converting them polar to cartesian coordinates. For SBI, we also include the two parameters ra_0 and dec_0 for the shear, which are always set to 0 when generating the training data sets, but in general our network could infer other values. Overall, there are 23 parameters for v_θ , which fully describe the simulation setup. However, in our dataset there are only 17 free parameters. The MCMC methods only infer the reduced set of parameters, making use of the dependencies between them.

Measurement instruments Observations have 160 times 160 pixels. The pixel size is 0.04 arc seconds. We use a Gaussian points spread function (PSF) with full width at half maximum (FWHM) of 0.3. There is Gaussian background noise with a root mean-squared values of 0.01 and an exposure time of 1000s.

Setup of MCMC-based methods We setup both baselines methods as follows:

1. Hamiltonian Monte Carlo: we use the No-U-Turn samples with a maximum tree depth of 10 and 5 000 warmup steps.
2. Affine-Invariant Ensemble Sampling: we use DEMove and StretchMove both with probability 0.5. There are 400 chains and we warm up for 20 000 steps before starting sampling.

Both methods are implemented in numpyro and optimized with JAX, so their runtimes are comparable with each other.

Network architectures and training

- Our flow network v_ϕ comprises a lightweight feature extraction network, represented by a CNN, which consists of 6 downsampling blocks with 1 layer each a 32 channels and kernel size 3. As postprocessing of the output, we apply GroupNorm, silu and an additional 2DConv layer with kernel size 3 and a single channel. We reshape the output and feed it through a final dense layer. The output of the feature extraction has the same dimensionality as the parameters θ .
- An additional dense feed-forward neural network receives the concatenated the time t , θ_t and extracted features as input. The feed-forward neural neural networks consists of 8 residual blocks with hidden dimension 128 and elu activation.
- The control network v_ϕ^C is represented by a small feed-forward neural network, consisting of 3 residual blocks with 64 hidden layers and 3 residual blocks with 32 hidden layers. We condition each block on the time via gated linear units and use a 16 dimensional time embedding.

For training, we use a batch size of 256 for the flow network v_ϕ . When training v_ϕ^C , we decrease the batch size to 16. We use the Adam optimizer with a learning rate of 10^{-4} and weight decay of 10^{-5} .

Table 4: Priors for lens mass model parameters

Parameter	Prior
x_{center}	$\mathcal{U}(-0.2, 0.2)$
y_{center}	$\mathcal{U}(-0.2, 0.2)$
position angle ϕ	$\mathcal{U}(0, 180)$
axis ratio q	$\mathcal{U}(0.25, 1)$
external shear orientation ϕ_{ext}	$\mathcal{U}(0, 180)$
external shear strength γ_{ext}	$\mathcal{U}(0, 0.1)$
Einstein radius θ_E	$\mathcal{U}(0.5, 2.0)$

Table 5: Priors for the source light

Parameter	Prior
amplitude	$\mathcal{U}(5.0, 10.0)$
half-light radius	$\mathcal{U}(0.5, 2.0)$
Sersic index n	$\mathcal{U}(1.5, 4.0)$
position angle ϕ	$\mathcal{U}(0, 180)$
axis ratio q	$\mathcal{U}(0.25, 1)$
x_{center}	$\mathcal{U}(-0.2, 0.2)$
y_{center}	$\mathcal{U}(-0.2, 0.2)$

Table 6: Priors for the lens light

Parameter	Prior
amplitude	$\mathcal{U}(5.0, 10.0)$
half-light radius	$\mathcal{U}(0.5, 2.0)$
Sersic index n	$\mathcal{U}(1.5, 4.0)$

Training v_ϕ was done on a single NVIDIA Ampere A100 GPU for ca. 45 hours. We trained v_ϕ^C for an additional 24 hours. A lot of the training time was spent on running evaluation metrics, so it can be substantially improved.

C.1 DIFFUSION POSTERIOR SAMPLING (DPS)

We setup diffusion posterior sampling Chung et al. (2023a) as an additional baseline. The training dataset is the same as in 6, however since the diffusion model is unconditional, we drop any conditioning information.

Network architecture and training The neural network architecture is a multilayer perceptron MLP with 8 residual blocks and 128 neurons each. The activation function is *elu*. As optimizer, we use Adam with weight decay (10^{-5}). We train for 2000 epochs and for each epoch we sample 1000 batches from the dataset using a batch size of 4. We train the network as a denoising diffusion probabilistic model (DDPM) following Ho et al. (2020).

Unconditional generation Below, in figure 11, we visualize three samples generated by unconditionally sampling from the model. The observations are created using the lensing simulation code with the generated samples as input.

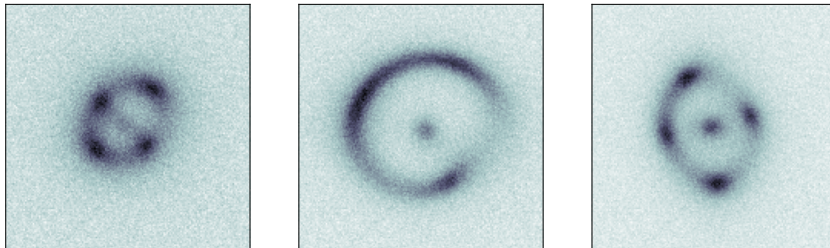


Figure 11: Visualization of unconditionally generated lensing systems.

Inference We directly follow Chung et al. (2023a) Algorithm 1 for inference, where the measurement operator \mathcal{A} is replaced by the lensing simulation code. The step size in the algorithm is defined via a hyperparameter ζ , which needs to be finetuned depending on the problem. We empirically test different values for ζ to find an optimal choice. Our results are shown in table 7. In this evaluation, we only model a smaller number of systems ($n = 25$).

ζ	0.0	0.0005	0.001	0.005	0.01	0.05
Avg. χ^2	28.15	16.20	9.98	10.07	12.98	12.64
Min. χ^2	15.14	3.84	3.07	1.58	1.40	1.53

Table 7: Evaluation of DPS and choosing ζ .

C.2 SIMULATION-BASED CALIBRATION

We use simulation-based calibration (Talts et al., 2018, SBC) as an additional evaluation method to assess the correctness of the posterior distributions. We adopt the SBC implementation from the Python package *sbi*. Below, in fig. 12, we show histograms for 8 parameters based on $n = 1000$ lens systems with $L = 1000$ posterior samples each.

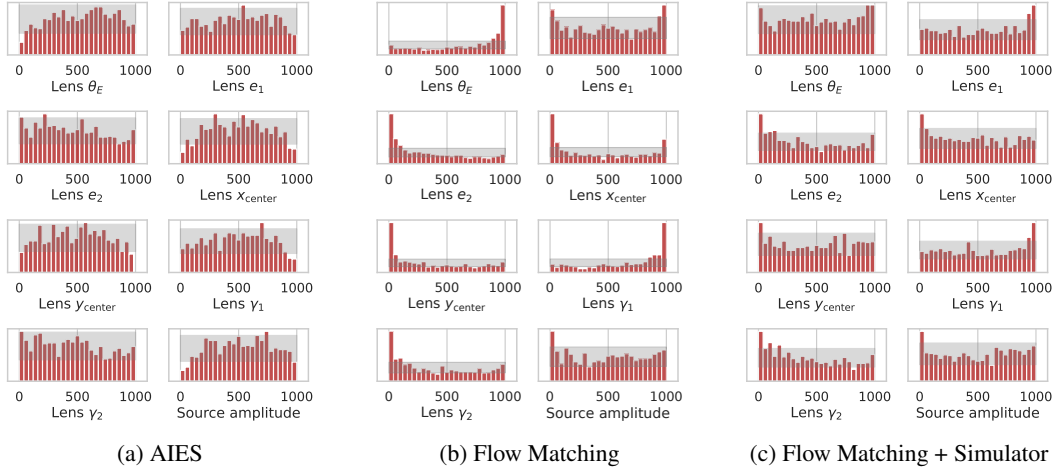


Figure 12: Simulation-based calibration histograms for different inference methods.

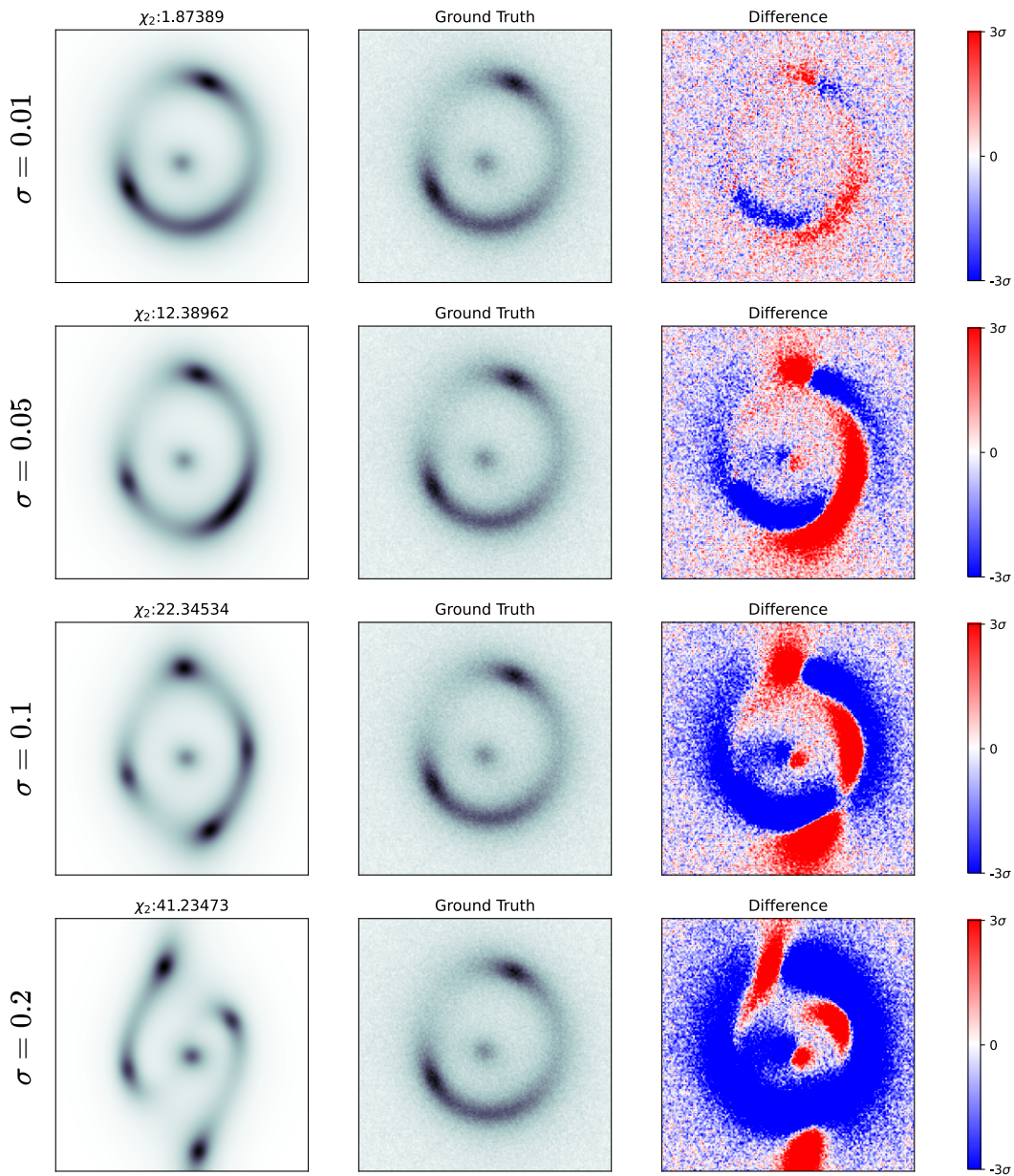


Figure 13: We show how a small noise σ affects the simulated observation. We add a normal Gaussian with mean 0 and standard deviation σ to a lens system's ground truth parameters x . Then, we plot the simulated observation based on the noised parameters and show the residuals.

D POSTERIORS AND RECONSTRUCTIONS FOR LENS MODELING

We show how small perturbations in the lens system's parameters affect the simulated observation in figure 13. We show extended plots of the posteriors in fig. 14 for lens system 1 and fig. 15 for lens system 6. Additionally, we show reconstructions based on flow matching with and without simulator feedback of lens systems 1 to 6 in fig. 16

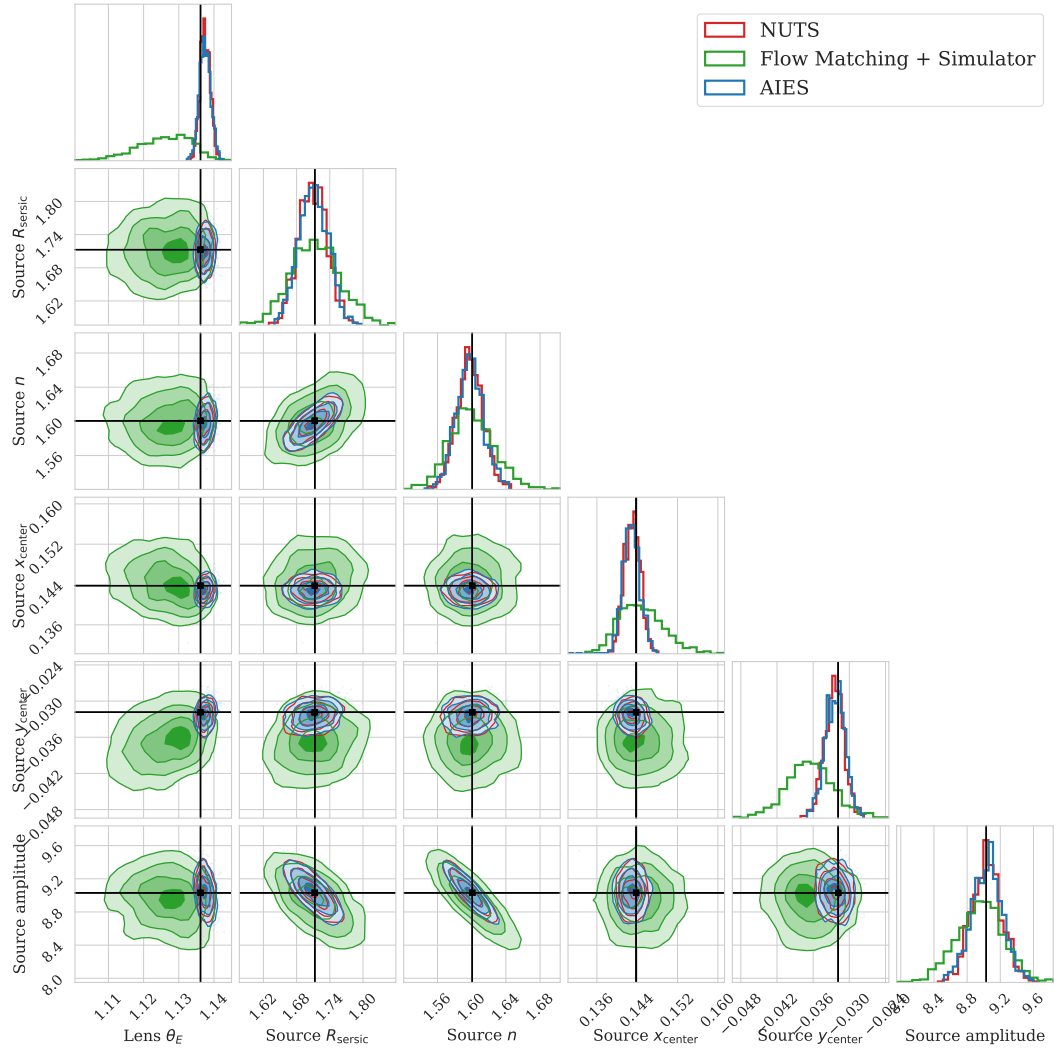


Figure 14: Posterior plot for system 1.

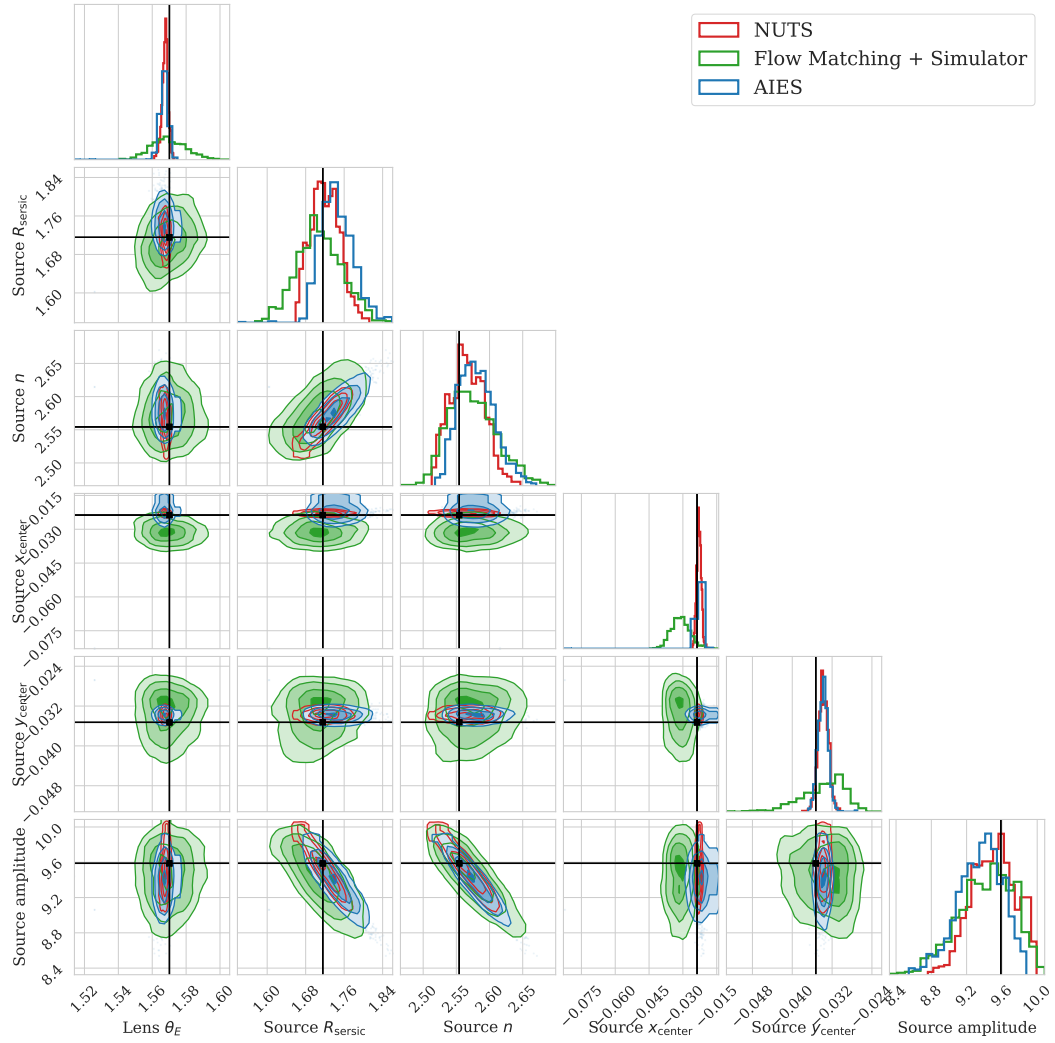


Figure 15: Posterior plot for system 6.

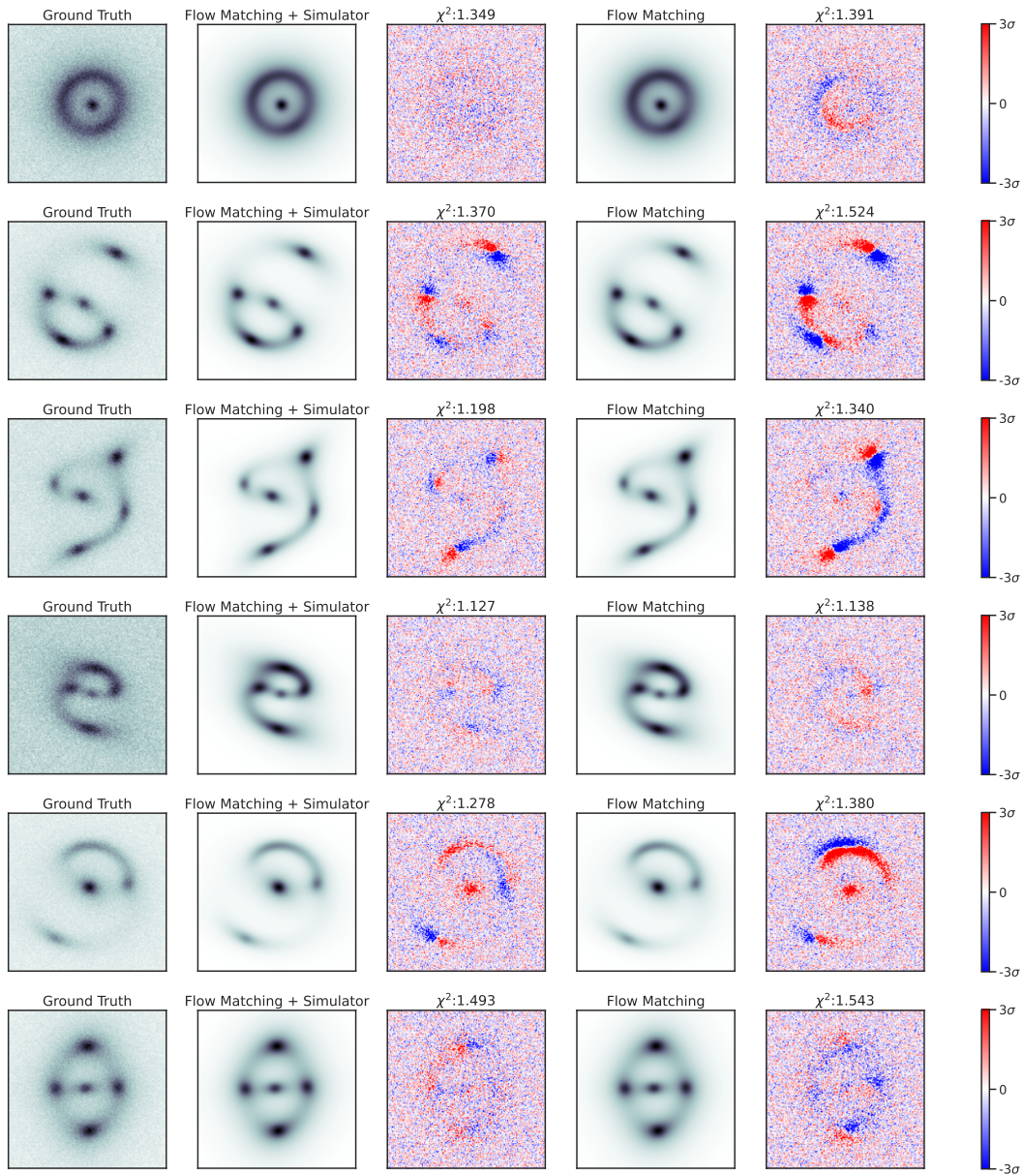


Figure 16: Modeling of different lens systems: system 1 (top) to system 6 (bottom).